Digital holographic microscopy is suitable for lipid accumulation analysis in single cells of Yarrowia lipolytica

Briel, Simon Carl Philipp; Feuser, Nicolas; Moldenhauer, Eva Johanna; Kabisch, Johannes; Neubauer, Peter; Junne, Stefan

Published in:
Journal of Biotechnology

DOI (link to publication from Publisher):
10.1016/j.jbiotec.2024.11.011

Publication date:
2025

Document Version
Publisher's PDF, also known as Version of record

Journal of Biotechnology 397 (2025) 32–43

Contents lists available at ScienceDirect

Journal of Biotechnology

journal homepage: www.elsevier.com/locate/jbiotec

Digital holographic microscopy is suitable for lipid accumulation analysis in single cells of *Yarrowia lipolytica*

Simon Carl-Philipp Briel [a], Nicolas Feuser [a], Eva Johanna Moldenhauer [b], Johannes Kabisch [c], Peter Neubauer [a], Stefan Junne [a,d,*]

[a] Technische Universität Berlin, Department of Biotechnology, Chair of Bioprocess Engineering, Berlin, Germany
[b] Technische Universität Darmstadt, Department of Biology, Computer-Aided Synthetic Biology, Darmstadt, Germany
[c] NTNU Norwegian University of Science and Technology, Department of Biotechnology and Food Science, Gløshaugen, Norway
[d] Aalborg University, Department of Chemistry and Bioscience, Esbjerg, Denmark

ARTICLE INFO

Keywords:
Oleaginous yeast
Food production
Process analytical technology
Fed-batch
Long-chain fatty acids

ABSTRACT

Digital holographic microscopy (DHM) is a label-free analytical technique for the determination of the cells' volume and their cytosolic refractive index. Here, we demonstrate the suitability of DHM for the quantification of total lipid accumulation in the oleaginous yeast *Yarrowia lipolytica*. Presently, microbial lipids are gaining increasing attention due to their nutritional value in feed and food applications. Their microbiological synthesis in algae and yeast is subject to optimization studies, which necessitates rapid quantification of total lipids for faster progress and the possibility of process control. So far, quantification of the total intracellular long-chain fatty acid concentration in yeast cells is time-consuming though when common chromatography for a volumetric analysis or staining and flow cytometry for a single-cell based analysis are used. This study, however, demonstrates that 3D-DHM facilitates a quasi-real-time measurement that allows for a rapid quantification of total intracellular lipid accumulation on a single-cell level without cell staining. Data from wild-type and lipid overproducing *Y. lipolytica* strains with specific yields of long-chain fatty acids in a range between 70 and 360 mg/gCDW show a good correlation with the optical volume determined by DHM, as the total lipid accumulation in the cell is typically well correlated with the long-chain fatty acid concentration. The results further correlate with data obtained from gas chromatography and flow cytometry of Nile Red-stained cells, which proves the reliability of DHM for lipid quantification in *Y. lipolytica*.

1. Introduction

Oleaginous microorganisms (yeasts, moulds and algae) have gained interest not just recently - the concept of commercially exploiting these as a source for oils and fats dates to the beginning of the last century (Ratledge and Wynn, 2002b). The production of microbial lipids has been studied thoroughly in the past (Taeuber et al., 2021; Lei et al., 2024). Polyunsaturated fatty acids (PUFAs) are interesting due to their widespread use as nutraceuticals (Sokoła-Wysoczańska et al., 2018) and biofuels (Junne and Kabisch, 2017). Cells are considered as oleaginous if they possess the potential to accumulate lipids to over 20 % (w/w) of dry cell mass (Thorpe and Ratledge, 1972). The main component of these microbial lipids are triacylglycerols (TAGs) together with free fatty acids, sterols and polar fractions (e.g. phospholipids, sphingolipids, glycolipids). The composition depends primarily on the carbon and nitrogen availability (Papanikolaou and Aggelis, 2011; Ratledge, 1993, 1994; Ratledge and Wynn, 2002b). The yeast *Yarrowia lipolytica* is known to be one of the most frequently applied hosts among oleaginous microorganisms, e.g. for PUFAs (Yan et al., 2024) and biofuels (Blazeck et al., 2014; Rakicka et al., 2015). They incorporate esterified fatty acids (FAs) mostly in non-polar TAGs (> 90 %) through the Kennedy pathway (Beopoulos et al., 2009; Kennedy, 1961). Hence, TAGs are the major part of storage lipids in *Y. lipolytica* in contrast to polar fractions (Papanikolaou and Aggelis, 2011). Its role as a model organism for biolipid production (Rakicka et al., 2015) relies on the FDA-assigned GRAS status (Xie et al., 2015), its wide substrate spectrum, and ease of genetic modification, respectively (Rakicka et al., 2015). Wild-type strains mainly produce C16 and C18 fatty acids when growing on glucose or glycerol, in a process known as *de novo* lipidogenesis (Kamineni and Shaw, 2020). Major constituents of these are palmitic

* Correspondence to: Aalborg University, Department of Chemistry and Bioscience, Niels Bohrs Vej 8, Esbjerg DK-6700, Denmark.
E-mail address: sju@bio.aau.dk (S. Junne).

https://doi.org/10.1016/j.jbiotec.2024.11.011
Received 30 July 2024; Received in revised form 12 November 2024; Accepted 13 November 2024
Available online 17 November 2024

acid (C16:0) and oleic acid ($^{\Delta 9}$C18:1). The latter contributes typically to about half of the total lipids. These are often esterified to > 90 % in TAGs (Papanikolaou and Aggelis, 2011). Next to the production of linoleic acid ($^{\Delta 9,12}$C18:2), most recent reports also give evidence of a non-negligible accumulation of linolenic acid ($^{\Delta 9,12,15}$C18:3) in wild-type *Y. lipolytica* strains (Carsanba et al., 2020).

To meet cost efficiency for microbial lipid production, strain selection and rapid process optimization play an increasing role, partly based on parallel cultivation (Patel et al., 2018). Rapid and accurate qualitative analysis and quantification of microbial lipids often rely on volumetric measurements, like the well-established gas chromatography (GC). Currently, other volumetric methods like near-infrared spectroscopy (NIRS) were proven to be well applicable (Chmielarz et al., 2019). Raman microscopy in liquid extracts of previously Deuterium-fed *Y. lipolytica* cell extracts (Kukal et al., 2022; Omelchenko et al., 2023), measured the ratio of unsaturated to saturated fatty acids *off line* in suspension samples of the yeast *Metschnikowia* spp. (Němcová et al., 2021).

Flow cytometry (FCM) can be regarded as a standard *at line* method to gain information on a single-cell level. It is suited for the identification of subpopulations in a microbial culture (Patel et al., 2019), but laborious and error-prone due to staining. Nevertheless, it has been applied successfully in combination with Nile Red or BODIPY® 505/515 staining for *in vivo* quantification of microbial lipids in microalgae (Cooper et al., 2010; De la Hoz Siegler et al., 2012; Encarnação et al., 2018; Govender et al., 2012; Rumin et al., 2015). Further, lipid droplet (LD) content analysis in various fission and budding yeasts is described with BODIPY® 493/503 staining of LDs in combination with 3D fluorescence microscopy and a following, automated image detection process (Princová et al., 2019).

Aside from flow cytometry, coherent anti-Stokes Raman scattering (CARS) confocal microscopy was applied at the single-cell level (Wolinski et al., 2012; Wolinski and Kohlwein, 2015). The possibility to quantify the lipid body fraction with Raman spectroscopy on slides with dried cell suspension is described in literature (Kochan et al., 2018). *In line* Raman spectroscopy is applied to quantify the total lipid fraction in *Cutaneotrichosporon oleaginosus* (Wieland et al., 2021). Raman-based analysis still requires expensive equipment (Gupta et al., 2019), statistic and further modelling for data extraction (Esmonde-White et al., 2022), although it represents a promising technique. Magnetic resonance imaging (MRI) and spectroscopy (MRS) are other examples of label-free lipid detection methods, which also require the presence of highly elaborated and yet non widely applied instruments though (Gupta et al., 2019; Hwang and Choi, 2015). Microscopy without the need of staining could be a simple alternative, yet most cells appear transparent or induce only small changes in the amplitude of light when accumulating lipids. This impairs the employment of conventional brightfield microscopy for the evaluation of lipid accumulation (Rappaz et al., 2014). Nevertheless, lipids cause a phase shift on transmitted light, which can be exploited by using spectrometric techniques. Therefore, a technique of special interest is 3D digital holographic microscopy (3D-DHM), which exploits the absorption of light from a light emitting diode of particles in comparison to a reference beam that passes through the sample towards a photodetector. It determines the cellular size, volume and phase homogeneity among other parameters. It is used for lipid quantification in adipocytes (Campos et al., 2018) and, under consideration of the cell diameter, in heterotrophically cultivated microalgae (Lemoine et al., 2017; Marbà-Ardébol et al., 2017). 3D-DHM is successfully applied to assess the lipid content inside the diatom *Phaeodactylum tricornutum* with a focus on the size of the liquid droplet (Yourassowsky et al., 2024). Reports describe the label-free quantification of intracellular osmolarity and cell volume in *Saccharomyces cerevisiae* by means of a digital holographic microscope, combined with a millifluidic chip (Boltyanskiy et al., 2022; Midtvedt et al., 2019). Recently, machine-learning assisted holographic microscopy was successfully applied in a beer yeast cell suspension with a moving window background subtraction. Classification of four metabolic states for each individual yeast with respect to growth activity is described (Sanborn et al., 2023). Nevertheless, there is no report of employing successfully 3D-DHM for lipid quantification in yeast so far. Therefore, this study evaluates the possibility of using 3D-DHM for rapid quantification of total lipids in *Y. lipolytica* wild-type and a genetically engineered strain during aerated batch and nitrogen-limited fed-batch bioreactor cultivations with glycerol as main carbon source.

2. Materials and methods

2.1. Yeast strains

Y. lipolytica (S11070) was used as representative for a wild-type strain as described previously in detail in (Hackenschmidt et al., 2019) as strain 63, described as strain S11070 by Bruder et al. (2020).

Follow-up studies in this work were conducted with a genetically engineered *Y. lipolytica* strain. The lipid overproducing strain S15010 with the genotype (*MATA ura3–302::SUC2 Δpox1–6 tgl4::pTEF-DGA1*) was created as follows: inspired by the work of (Blazeck et al., 2014), the gene *tgl4* which encodes a lipase of strain H222ΔP (Gatter et al., 2014), a knock-out strain deficient of six POX genes, was deleted by integrating a DNA cassette which contained the acyl-CoA:diacylglycerol acyltransferases isozymes II gene (*DGA1*) under control of the strong, constitutive TEF-promoter. The DNA for the knock-out/-in construct was assembled using transformation assisted recombination in *S. cerevisiae* strain BY4741. The assembled plasmid was amplified using *Escherichia coli* strain DH10B. It was linearized by cutting with *Stu*I and transformed into *Y. lipolytica* as described by Bruder et al. (2019).

2.2. Cell maintenance

Cells were firstly grown on YPD agar plates, which consisted of 1 % yeast extract, 2 % peptone, 2 % dextrose and 2 % agar (all w/w). For inoculation, a single colony was picked from the plate and transferred to 25 mL of liquid medium, then incubated at 30 °C and 250 rpm. Cells were grown in buffered YPD liquid medium with the composition as described above, omitting the agar. The medium was supplemented with 1.4 % KH_2PO_4 and 0.1 % $(NH_4)Cl$ as buffering agents according to (Maczek et al., 2006), titrated to pH 5.5 and used for cultivation of the cells in 500 mL glass shake flasks without baffles. Cells were harvested in the late exponential phase after incubation at 30 °C and 250 rpm. 1 mL of crude cell broth was mixed with 500 µL of 50 % (v/v) sterile aq. glycerol and immediately stored at −80 °C.

2.3. Bioreactor cultivation

All chemicals for media and analytical procedures were obtained from Carl Roth (Karlsruhe, Germany) if not separately mentioned. For bioreactor cultivations, a two-stage pre-culture was applied allowing the cells to adapt to the mineral salt medium. The first pre-culture was grown in buffered YPG medium, the same as buffered YPD medium. Dextrose was substituted by glycerol (final concentration of 1 % (w/w)), with an inoculum of 200 µL from a cryogenic stock. Cultivation parameters were the same as for cryogenic stock preparation. The culture was harvested after approximately 12 h at an OD_{600} of 13. It has been used for the inoculation of the second pre-culture. 50 mL of batch medium, as described below, was inoculated to reach an initial OD_{600} of 2. The culture was then grown to an optical density of $OD_{600} = 7$ at 30 °C and 250 rpm.

Stirred tank bioreactors KLF 2 (Bioengineering, Wald, Switzerland) were inoculated to reach a start OD_{600} of 0.15 in 2 L of batch medium (Bruder et al., 2019). The batch medium for cultivations contained: 30 g/L carbon source (glycerol), 0.5 g/L yeast extract, 1.1 g/L $MgSO_4*7H_2O$, 0.2 g/L $CaCl_2*6H_2O$, 0.5 g/L $MgCl_2*6H_2O$, 0.075 g/L myo-inositol, 1.36 g/L KH_2PO_4, 1.74 g/L K_2HPO_4, 0.2 mg/L

$CuSO_4$*5H_2O, 1 mg/L $FeSO_4$*7H_2O, 0.2 mg/L $MnCl_2$*4H_2O, 0.2 mg/L Na_2MoO_4*2H_2O, 0.2 mg/L $ZnSO_4$*7H_2O, 5 mg/L biotin, 100 mg/L D-pantothenic acid hemicalcium salt, 20 mg/L nicotinic acid, 60.8 mg/L pyridoxine hydrochloride, 20 mg/L thiamine hydrochloride and 5 g/L NH_4Cl. Feed medium for fermentation contained 400 g/L carbon source (glycerol), 3.3 g/L $MgSO_4$*7H_2O, 0.6 g/L $CaCl_2$*6H_2O, 1.5 g/L $MgCl_2$*6H_2O, 0.45 g/L myo-Inositol, 2.72 g/L KH_2PO_4, 3.48 g/L K_2HPO_4, 0.6 mg/L $CuSO_4$*5H_2O, 3 mg/L $FeSO_4$*7H_2O, 0.6 mg/L $MnCl_2$*4H_2O, 0.6 mg/L Na_2MoO_4*2H_2O, 0.6 mg/L $ZnSO_4$*7H_2O, 15 mg/L biotin, 300 mg/L D-pantothenic acid hemicalcium salt, 60 mg/L nicotinic acid, 182.4 mg/L pyridoxine hydrochloride, 60 mg/L thiamine hydrochloride and 0.01 g/L $FeCl_3$*6H_2O. Antifoam 204 (Sigma, Neustadt a. d. Weinstraße, Germany) was added to each bioreactor at a concentration of 1 mL/L before *in situ* media sterilization. The reactors were equipped with two Rushton turbines and *in situ* sterilized. Initial process parameters were pH = 6.3, temperature = 30 °C, aeration = 0.5 vvm and stirrer speed = 400 rpm. The pH-value was controlled at pH = 3.0 by adding 2 M NaOH. The agitation rate was increased up to 1, 200 rpm when the dissolved oxygen concentration (DO) fell below 20 % of saturation to ensure aerobic conditions. A pulse of feed medium (Bruder et al., 2019), according to 25 g/L of glycerol with respect to the initial batch medium volume, was supplied manually when the carbon source was depleted, as indicated by a sharp increase of the DO. 25 mL samples were taken every 2 h for the *off line* determination of OD, pH-value, cell dry weight (CDW), metabolites via high performance liquid chromatography (HPLC, enzymatic analysis with the Cedex Bio HT Analyzer (Roche Custom Biotech, Mannheim, Germany) and intracellular lipid content via gas chromatography and flow cytometry of stained cells.

2.4. Analytics

2.4.1. Cell growth and metabolites

Cell growth was quantified by measurement of the optical density at a wavelength of 600 nm with a spectrophotometer (Ultraspec 3000, GE Healthcare, Chicago, IL). For the *in line* monitoring of the cell density, the Dencytee sensor (Hamilton, Bonaduz, Switzerland) was applied. For analysis of the CDW, 2 mL of crude culture broth was centrifuged at 21,500 x g for 5 min and 4 °C, washed twice with 0.9 % (w/w) NaCl solution and centrifuged again under the same conditions. The pellets were dried at 80 °C for at least 24 h while the culture supernatant was filtered with a 0.2 µm PTFE filter (VWR International, Darmstadt, Germany) and stored at 4 °C prior to metabolite analysis.

Short-chain carboxylic acids were quantified with an Agilent 1200 HPLC system (Agilent Technologies, Ratingen, Germany), equipped with a refractive index detector and a HyperRez XP carbohydrate H^+ column (300 × 7.7 mm, 8 µm; Fisher Scientific, Schwerte, Germany). A 5 mM H_2SO_4 solution was used as eluent at a flow rate of 0.6 mL/min and a column temperature of 65 °C. The injection volume was 20 µL. For data analysis, Agilent ChemStation software, version 4.03 was applied.

The glycerol, ammonia and phosphate contents were determined enzymatically with a Cedex Bio HT Analyzer from the same samples as for HPLC analysis, following the kit instructions as specified by the manufacturer.

2.4.2. Lipid analysis

Long-chain fatty acid analysis was performed with a gas phase chromatograph equipped with a flame ionization detector as published by (Hillig et al., 2013) with a few modifications. Samples were adjusted to OD_{600} = 10 in a total volume of 20 mL, washed twice with cold de-ionised water, centrifuged (8,000 rpm, 10 min, 2 °C) and resuspended in 500 µL dried methanol. Internal standard (100 µL of 1 g/L nonadecanoic acid, dissolved in chloroform) and 2 mL of a 10:1 mixture of dried methanol and acetyl chloride was added to the samples, which were then incubated at 50 °C for 16 h in a water bath (all chemicals were obtained from Sigma). Methyl esters were extracted twice with 5 mL hexane (VWR, Darmstadt, Germany), shaken with a rotor driver for 15 min and dried with vacuum. The pellet was solved in 1.5 mL hexane, transferred to a GC vial and analyzed by a gas chromatography GC-2010 Plus (Shimadzu, Kyoto, Japan) equipped with a flame ionization detector. Temperature settings of the injector, column and detector were as follows: 290 °C, 150 °C and 300 °C, temperature gradient mode for the column started at 150 °C for 2 min, heating to 250 °C with a rate of 15 K/min, holding time 37 min, heating to 280 °C with a rate of 5 K/min, before the temperature was kept until the termination of the run. The separation was carried out on a 0.25 mm × 25 m polydimethylsiloxane (0.12 µm, CP-Sil 5 CB) capillary column (Varian, Darmstadt, Germany). Ultrapure nitrogen was used as carrier gas. The injection volume was 0.3 µL in splitless mode. The long-chain fatty acid composition was determined on the basis of retention times of known long-chain fatty acid methyl ester standard mixes (GLC-10, GLC-20, GLC-40, GLC-50; Merck, Darmstadt, Germany) containing the methyl esters of palmitate, palmitoleate, stearate, oleate, linoleate, linolenate and arachidate. Quantification was performed by the integration of the peaks with GC solution software version 2.2 (Shimadzu). The retention order was further investigated with GC-MS.

2.4.3. Cell staining and flow cytometry

Prior to flow cytometry analysis, 2 mL of culture broth was washed with 5 mL of phosphate buffer (8 g/L NaCl, 0.2 g/L KCl, 1.44 g/L Na_2HPO_4, 0.24 g/L KH_2PO_4, pH 7.2) via vacuum filtration with a filter of a pore size of 0.2 µm (Sartorius Stedim, Göttingen, Germany) directly after sampling, and resuspended in 10 mL of buffer. Samples were measured directly using a MACSQuant Analyzer (Miltenyi Biotec, Bergisch Gladbach, Germany) at an extinction wavelength λ_{ex} = 488 nm from an argon-ion laser source at 25 mW and detection at an emission wavelength λ_{em} = 580 nm. The cell density was adjusted between 10^6 and $5{\cdot}10^6$ cells/mL. Nile red (Sigma) staining for neutral lipid detection was performed by mixing 200 µL of diluted sample with 10 µL of Nile Red working solution (100 µg/mL in acetone) and incubation at 37 °C for 30 min in the dark (final Nile Red concentration of 5 µg/mL). For each analytical run, at least 50,000 events were measured in the gated part. For data evaluation, MACSQuantify™ version 2.11 (Miltenyi Biotec) and FlowJo™ version 10.7 (LLC, Ashland, USA) software was applied.

2.4.4. Microscopy

The 3D digital holographic microscope oLine-OT40GA (Ovizio, Brussels, Belgium) was used to monitor the alteration of the cells' optical parameters upon lipid production and accumulation throughout the course of the cultivation. Samples drawn from the bioreactor were diluted to OD_{600} = 1.0. 5 µL were directly applied on the microscope slide and measured. Several captures were taken at each time point to achieve at least 100 cell counts recognized by the OsOne software version 4.3 (Ovizio) at each individual measurement. The settings were adjusted for automated *Y. lipolytica* yeast cell detection and are summarized in Table 1. Object focus was conducted manually with the automated tray shift. A high portion of cells being only partly in focus or in the image array were avoided by manual eye control. Cell edges were used as reference points to achieve a suitable focus level. All other steps

Table 1
Parameters for automatic detection of *Y. lipolytica* yeast cells in the OsOne software version 4.3 (Ovizio, Brussels, Belgium).

Parameter	
Background	270
Median cell size [µm]	7.69
Background detection algorithm	Phase variance
Cell minimum size [pixels]	79
Noise removal filter	5
Split cell aggregates	5
Invalid area sensitivity	13

that followed image capture were automated. The image recognition was checked by eye for each case and withdrawn in case of bad recognition (non-distinguished cell borders, non-separated background). This was, however, only the case for a very few captures among all images that had been taken.

Parameters as in Table 1 were chosen on an empiric basis from preceding yeast cultivations and have been optimized for automated *Y. lipolytica* cell recognition and distinction from the background by a phase variance algorithm. Manual control of the processed images proved that incorrectly separated or false-positive detected cells constituted only a negligible, statistically non-relevant share of the total counts with this microscope parameter set. Exemplary images from different time points of the cultivation are provided in Fig. 1 for the assessment of the images' detection quality. Following cell recognition, optical parameters were automatically calculated for each single cell. The arithmetic mean, median and variance were then calculated for data at each time point and plotted over the total and specific long-chain fatty acid concentrations determined by GC-FID to identify potential correlations. For Pearson correlation analysis, OriginPro 2015 software (OriginLab, Northampton, MA) was used. As different background (reference) captures were used at cultivations with the wild-type and the genetically modified strain, values of the optical volume were normalized.

3. Results and discussion

In this study, the systematic investigation of 3D-DHM for intracellular lipid quantification on a single-cell basis is described for the oleaginous yeast *Y. lipolytica*. While being aware of other methods for lipid quantitation like coherent anti-Stokes Raman scattering (CARS) confocal microscopy (Wolinski et al., 2012; Wolinski and Kohlwein, 2015), magnetic resonance spectroscopy (Gupta et al., 2019; Hwang and Choi, 2015) or image-based cytometry, it is sought to evaluate an alternative method that is label-free, robust against media compounds and image-based.

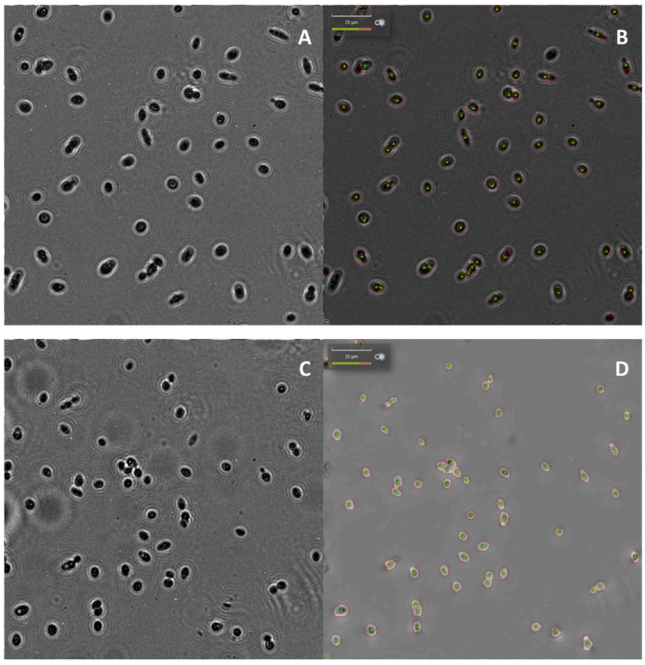

Fig. 1. : Images of diluted *Y. lipolytica* wild-type strain S11070 cultivation broth samples. Captures were taken with 3D digital holographic microscopy; the cell recognition algorithm was set to the parameters mentioned above (Table 1) for cell detection. Red circles are the segregation boundary of the cells from the background, green dots mark the recognized cell cores. Raw images are shown on the left side, processed images at the right side. Samples are from 36.38 h (A, B) and 64.88 h (C, D) after cultivation start. The scale shows a length of 20 μm.

Firstly, results of cultivations with the wild-type strain S11070 (Hackenschmidt et al., 2019) are used for a proof-of-principle approach to investigate whether 3D-DHM can give rise to quantitative data on the accumulation of total intracellular lipids from low quantities on. The results are subsequently verified with a genetically modified strain that is capable to achieve higher lipid titres, which is often an important pre-requisite for economic feasibility of microbial lipid production (Kamineni and Shaw, 2020). Finally, results of 3D-DHM are compared with those of established methods, i.e. GC and flow cytometry-based lipid quantification.

3.1. Two-stage repeated fed-batch cultivation

Results are obtained from two *Y. lipolytica* 2 L bench-top stirred-tank reactor cultivations as repeated fed-batch and a final optical density of about $OD_{600} = 100$. This corresponds to a cell dry weight of about 30 g/L (Fig. 2A, B). As the batch medium contains 5 g/L of ammonium chloride as nitrogen source while the feed does not contain any nitrogen, a distinction between two cultivation phases (nitrogen excess and nitrogen limitation) is achieved. Growth retardation due to nitrogen limitation is seen in the growth profiles (Fig. 2C, D): cells grow exponentially until 16.5 h before a linear growth stage is reached when ammonia is depleted. The main reason for the initial pH drop is the consumption of ammonia sources; the time course of the ammonia concentration proves this dependency. The feed is added repeatedly to a final concentration of 25 g/L glycerol in the cultivation broth every time the DO increases sharply (Bruder et al., 2019) in order to avoid long phases of a carbon-limited growth condition (Fig. 2C, D). The alternating carbohydrate availability impacts the O_2 and CO_2 concentrations in the off-gas (Fig. 2E, F). Phases of carbon source depletion lead to a reduction of metabolic activity, and thus a reduced oxygen demand, which is seen in off-gas O_2 concentrations (Fig. 2E, F). Throughout lipidogenesis, molecular oxygen is consumed for the production of long-chain fatty acids (Papanikolaou and Aggelis, 2011); thus, the oxygen concentration decreases in the off-gas. Acidification of the culture medium during that phase, after ammonia depletion (Fig. 2A, B), may partly be due to the synthesis of pyruvate and oxaloacetate, intermediates of *de novo* lipidogenesis from carbohydrate sources like glycerol (Evans et al., 1983; Ratledge and Wynn, 2002b).

The total intracellular long-chain fatty acid accumulation is increasing (Fig. 2I, J) exactly when ammonium becomes fully depleted (Fig. 2G, H). In fact, it is well-known that in case of *de novo* lipid production in oleaginous yeast, nitrogen limitation is important (González-García et al., 2017; Ratledge and Wynn, 2002b). Slightly different lipid concentrations are observed during the course of the wild-type strain cultivations with comparably low long-chain fatty acid formation rates over a long cultivation time. Nevertheless, this does not complicate the evaluation of DHM.

Short-chain carboxylic acids, in particular lactic, acetic, citric and pyruvic acid hardly accumulate during the cultivations, the first three remained below the detection threshold of about 0.1 μM (data not shown) – as measured via HPLC and enzymatically in supernatant samples. *Y. lipolytica* obviously consumed mitochondrial-derived, cytosol-relocated citric acid for ATP-citrate lyase-driven acetyl-CoA production and ultimately cytosolic storage of long-chain fatty acids (Boulton and Ratledge, 1981; Dulermo et al., 2015). ATP-citrate lyase (ACL) is highly active in wild-type *Y. lipolytica* during the lipidogenetic phase, which poses the explanation for the absence of any citric acid despite the continuing bolus feeding of carbon source (Ochoa-Estopier and Guillouet, 2014). Pyruvic acid accumulates up to concentrations of 0.1 g/L in the cultivation medium, but only during exponential growth (Fig. 2G, H), before the N-source is depleted prior to lipid production. This, however, is not surprising as *Yarrowia* sp. are known to be deficient of a cytosolic variant of the malic enzyme (ME) (Zhang et al., 2013).

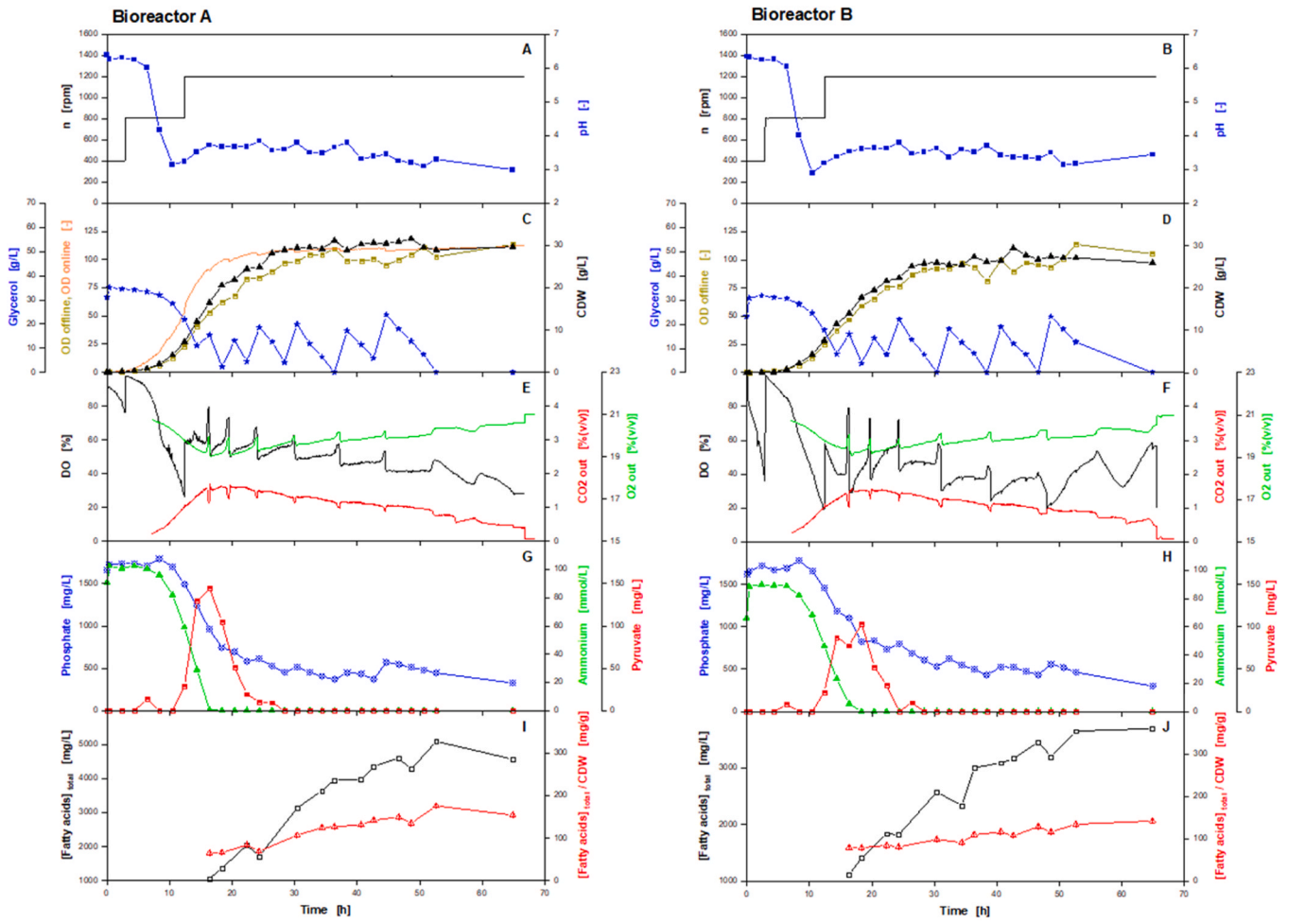

Fig. 2. : Two-stage repeated fed-batch cultivation of the oleaginous yeast *Yarrowia lipolytica* wild-type strain S11070 in a mineral medium inside two 2 L bench-top stirred tank reactors (biological duplicate). The feed contains glycerol, but no nitrogen source, and was manually added to a final concentration of 25 g/L in the fermentation broth every time the dissolved oxygen (DO) increased sharply, as a sign of a primary carbon source depletion. The pH value was adjusted to $pH_{start} = 6.3$ and subsequently regulated to pH = 3.0 with 2 M NaOH.

While *Y. lipolytica* possesses a mitochondrial variant of ME – also converting L-malate to pyruvate – it is likely not involved in NADPH regeneration for fatty acid synthesis (Zhang et al., 2013). Mitochondrial ME is not required for lipidogenesis (Dulermo et al., 2015). Hence, pyruvic acid is not produced from a putative ME-catalysed reaction.

3.2. Lipid accumulation analyzed with gas chromatography

In the following, results of GC-FID analysis as 'golden standard' for volumetric lipid analysis will be discussed for the comparison with data from other analytical methods. Analysis will be restricted to the long-chain fatty acids being accumulated by the wild-type strain, which are mainly oleic acid ($^{\Delta 9}$C18:1), linoleic acid ($^{\Delta 9,12}$C18:2), palmitic acid (C16:0) and palmitoleic acid ($^{\Delta 9}$C16:1) (Kyle et al., 1992; Papanikolaou and Aggelis, 2011, 2009) and fewer amounts of linolenic acid ($^{\Delta 9,12,15}$C18:3) as observed in *Y. lipolytica* wild-type strains (Carsanba et al., 2020). Oleic, linoleic and linolenic acid are shown as one total value (Fig. 3D), because of an uncertain separation of peaks by GC-FID, due to the compounds' similar chemical structure and as any separation is not of foremost interest for this work.

Sampling for fatty acid quantification was started after approximately 16.5 h post inoculation, exactly when ammonia becomes depleted in the culture medium (Fig. 2G, H). For both, bioreactor cultivations A and B, the time courses of long-chain fatty acid accumulation show a similar development. Critical points like the entrance into another cultivation phase at 50 h are identical and indicate a good comparability between both cultivations. The total values differ while in bioreactor cultivation B, a consistently lower concentration of all long-chain fatty acids is observed. This is seen as typical variation when cultivating wild-type strains of oleaginous yeast in biological replicates as previously mentioned. Detailed information about the total amounts of long-chain fatty acids and their respective distributions are displayed in Table 2.

For comparison with other work, a conclusive overview on different carbon sources utilized for *Y. lipolytica* wild-type cultivations and their respective yields in long-chain fatty acids are summarized in Table 3. In case of growth on hydrophilic carbon sources like glucose or fructose, specific maximum yields of total lipids are in the same range, i.e. between about 50–200 mg/g_{CDW}. This finding substantiates the usefulness of the bioreactor cultivation experiments in this work as a basis for subsequent intracellular lipid analysis.

3.3. Flow cytometry with Nile Red staining

To corroborate the results of the precedingly performed GC analysis of intracellular lipids, FCM was employed in combination with Nile Red staining of intracellular LDs (Delvigne et al., 2018). Volumetric analysis techniques like GC may be complemented by single-cell analysis for an increased information content. For validation, the results of GC and FCM are correlated. This serves as a starting point for the subsequent

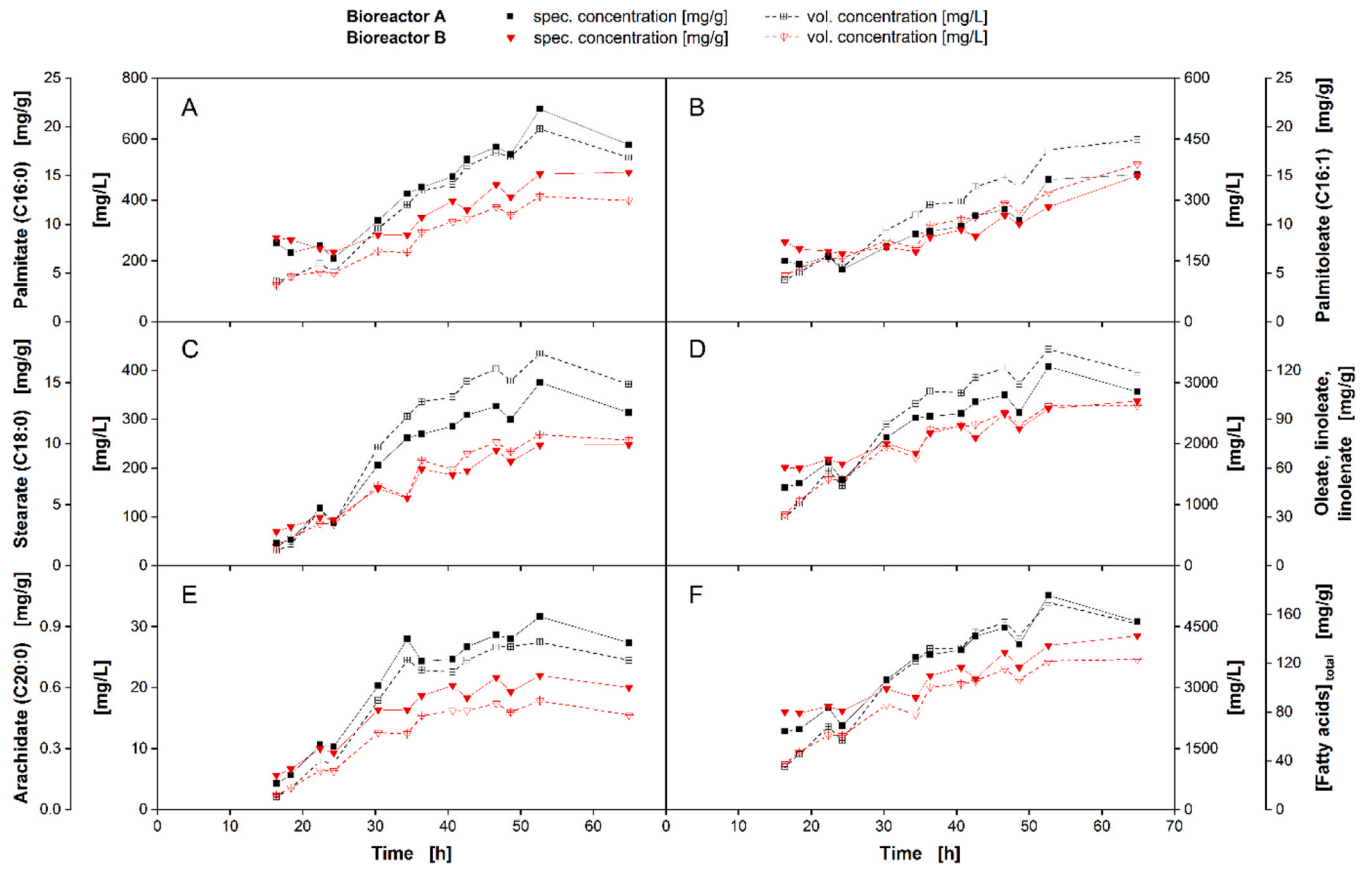

Fig. 3. : Lipid accumulation over the cultivation time course in *Y. lipolytica* S11070 cultivations. The graphs are separated for bioreactor A (black) and bioreactor B (red), specific fatty acid concentration is indicated by solid line with filled symbols and volumetric concentration by dashed line and empty symbols. The most prominent long-chain fatty acids are displayed, which are palmitate (A), palmitoleate (B), stearate (C), oleate, linoleate and linolenate (D), arachidate (E) as well as the total long-chain fatty acid concentration (F).

Table 2
Overview of intracellular long-chain fatty acids produced in *Y. lipolytica* S11070 fed-batch cultivations corresponding to Fig. 3 as measured in late samples (~65 h after inoculation). Values are displayed in volumetric concentration [mg/L] with respect to the total working volume and specific concentration [mg/g_{CDW}], respectively.

Fatty Acid	Reactor A [mg/L]	Reactor A [mg/g_{CDW}]	Reactor B [mg/L]	Reactor B [mg/g_{CDW}]
Palmitic acid (C16:0)	539	18.2	398	15.4
Palmitoleic acid (C16:1)	448	15.1	389	15.0
Stearic acid (C18:0)	372	12.5	257	9.90
Oleic, linoleic, linolenic acid (C18:1–3)	3172	107	2624	101
Arachidic acid (C20:0)	24.50	0.80	15.50	0.60
Total long-chain fatty acid concentration	4573	154	3696	143

Table 3
Overview of long-chain fatty acid yields at different carbon sources for *Y. lipolytica* wild-type strains.

Carbon source	Cultivation mode (cultivation vessel, vessel volume, feed, temperature)	Max. lipid content [mg/g_{CDW}]	Source
Glycerol	Bioreactor, 2 L, Bolus feed, 30 °C	154	this work
Glucose	Bioreactor, 5 L, Batch, 28 °C	120	Lazar et al. (2014)
Fructose	Bioreactor, 5 L, Batch, 28 °C	90	Lazar et al. (2014)
Glucose	Shake flask, 200 mL, Batch, 28 °C	180	Kolouchová et al. (2016)
Glucose	Shake flask, Batch, 28 °C	30–450	Carsanba et al. (2020)
Glucose	Shake flask, 50 mL, Batch, 28 °C	57	Beopoulos et al. (2008)
Oleic acid (60 %)		128	Beopoulos et al. (2008)
Oleic acid (98 %)		315	Beopoulos et al. (2008)

correlation of 3D-DHM results to both GC-FID and FCM analyses.

From shortly before nitrogen depletion onwards (Fig. 2G, H), samples were taken for cytometric analysis. Results of flow cytometric measurements regarding intracellular lipid accumulation are shown in Fig. 4. The degree of population heterogeneity is determined by the standard deviation of Nile Red fluorescence intensity in each sample. Gating of measurements was employed to exclude parts of lysed cells and media components. At least 50,000 events per sample were measured in the gated part to ensure statistical relevance. All samples were measured in triplicate, both stained with Nile Red (exemplarily shown in fig. A1 in the appendix) and unstained as a negative control. Stained cells showed an increasing fluorescence signal at λ_{ex} = 488 nm (suitable for Nile Red detection in yeast (Lorenz et al., 2017)) over the cultivation time, both equally in bioreactor A (upper row) and bioreactor B (lower row), visualizing the increasing intracellular lipid content (Fig. 4). An overview over all values is given in Table 4.

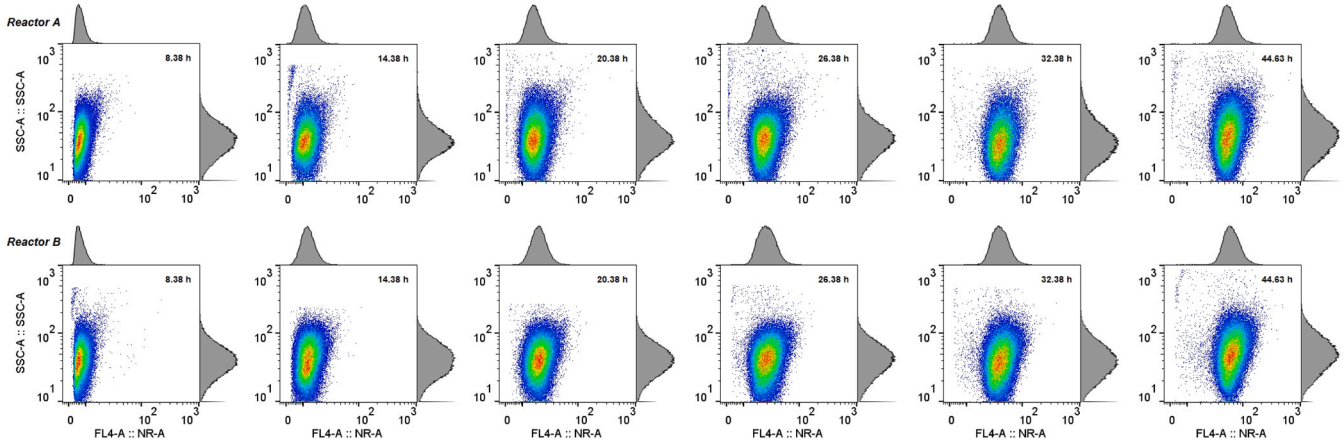

Fig. 4. : Intracellular lipid accumulation over the course of cultivations as captured by flow cytometry of Nile Red-stained *Y. lipolytica* S11070 cells. Fluorescence was measured at an excitation wavelength of λ_{ex} = 488 nm and emission wavelength of λ_{em} = 580 nm, displayed by the heat maps. An increase in the fluorescence intensity of Nile Red indicates intracellular lipid storage. The side scatter (cell granularity) and forward scatter (cell size) are indicated by the histograms attached to each diagram on the y-axis and x-axis, respectively. Every sample was measured in triplicate. All measurement events were gated to exclude artefacts. Upper row is bioreactor A, lower row is bioreactor B. The following samples were examined: column 1: 8.38 h, column 2: 14.38 h, column 3: 20.38 h, column 4: 26.38 h, column 5: 32.38 h, column 6: 44.63 h. SSC-A: side scatter area, FL4-A: fluorescence channel 4, NR: Nile Red. Results are shown from the gated part exclusively. Gating was performed to include almost all particles from cellular origin in the analysis.

Table 4
Results of flow cytometry analysis of Nile Red-stained *Y. lipolytica* S11070 cells. Samples were measured in triplicate, a minimum of 50,000 detection events were analyzed per sample. Fluorescence intensity is given in arbitrary units and the arithmetic mean is calculated for each sample, as it is a measure for intracellular lipid concentration. The standard deviation is a measure for population heterogeneity (with respect to intracellular lipid accumulation). Results are shown from the gated part exclusively. Gating was performed to include almost all particles from cellular origin in the analysis.

	Bioreactor A Fluorescence signal at λ_{em} = 580 nm		*Bioreactor B Fluorescence signal at λ_{em} = 580 nm*	
Time [h]	**Arithm. mean μ [-]**	**Std. deviation σ [-]**	**Arithm. mean μ [-]**	**Std. deviation σ [-]**
8.38	7.33	3.08	7.37	3.55
14.38	12.7	5.52	14.4	5.63
20.38	20.5	8.16	24.6	8.46
26.38	29.8	11.0	32.4	11.6
32.38	46.9	14.6	47.3	15.9
44.63	62.2	20.6	70.1	23.5

The increasing fluorescence intensities (arithmetic mean) during the course of the cultivations are a clear indication that cells are accumulating lipids (Fig. 4), in good agreement with GC analysis (Fig. 3). A further proof is the increasing light absorption as determined by the forward scatter of FCM (Fig. 4, shown as histograms on the upper x-axis in each diagram), that can be partly ascribed to the accumulation of intracellular lipids, that is a change of cell volume and optical features. As it is typical for long cultivation periods, a distribution of the cell age evolves together with an increase of population heterogeneity. As seen in Table 4, between cultivation times of 8.38 h and 44.63 h, the standard deviation of Nile Red fluorescence intensity increases from ~3 % to >20 % in both bioreactors. This can be observed at a broader distribution of the fluorescence intensity (x-axes of heat maps in Fig. 4). In addition, the side scatter, a measure for cell interior optical features, is also increasing during bioreactor cultivations (Fig. 4, shown as histograms on the right y-axes). In case lipid droplets increase inside a cell, the density, and thus the side scatter is altered. Nile Red is a solvatochromic stain which is known to shift its absorption wavelength and emission maximum in dependency of the pH of its environment (Greenspan and Fowler, 1985). In fact, the pH value of the cultivation broth was actively regulated and kept constant at pH = 3.5. Samples were immediately washed and buffered to neutral pH =7.2, which made the samples comparable with each other due to similar processing. Nile Red incorporates to neutral lipids in LDs and phospholipids that are constituents of microbial membranes. In turn, lipid-containing compartments are proportionally detected in dependence of their relative share of the cells' total lipids. Additionally, emission wavelength maxima for Nile Red-labelled compartments are different – for instance an increased LD amount causes a blue shift of the Nile Red emission wavelengths (Wolinski and Kohlwein, 2008). Consequently, the intensities as a measure for the (specific) lipid content in Nile Red-stained yeast depend on the selected emission wavelength (Kimura et al., 2004). Absorption wavelength shifts for reasons exceeding the taken precautions may not seem relevant in the scope of this work which is proven by a good correlation with results of GC measurements (Fig. 5). Pearson analysis indicates a positive correlation with coefficients of $r > 0.98$ for both bioreactor cultivations. The p value proves statistical relevance ($p < .003$).

The strong positive correlation between results from GC-FID and FCM demonstrates Nile Red staining and fluorescent read-out at λ_{em} = 580 nm to suffice the accuracy needed for reliable lipid quantification as relevant for this work. It is, however, foremost for the above-mentioned reasons that we aim to evaluate 3D-DHM as an alternative label-free and simple method that might circumvent the added effort and error sources associated with staining methods.

3.3.1. *Lipid accumulation analyzed with 3D-DHM*

3D-DHM allows to follow the same parameter set as with FCM which was previously described, i.e. cell size/volume and cell granularity, but with significantly less workload and processing time. Therefore, this study aims to demonstrate the applicability of 3D-DHM for monitoring the accumulation of intracellular lipids in oleaginous yeast on a single-cell level and label-free. The automated image recognition was fully repeatable under the given parameter set (Table 1). In the following section, GC-FID and FCM are compared to quantitative data acquired by 3D-DHM with simple regression to identify any obvious and consistent correlation. As a proof-of-principle approach, the same samples used for GC and FCM analyzes were applied for 3D-DHM. In comparison to the first two methods, liquid handling was limited to pipetting 5 μL of crude fermentation broth, diluting it to 100-fold in 0.9 % (w/w) NaCl solution, and directly exposing the sample to microscopy. The total processing time to capture and fully recognize cells on images took 300 s for 100

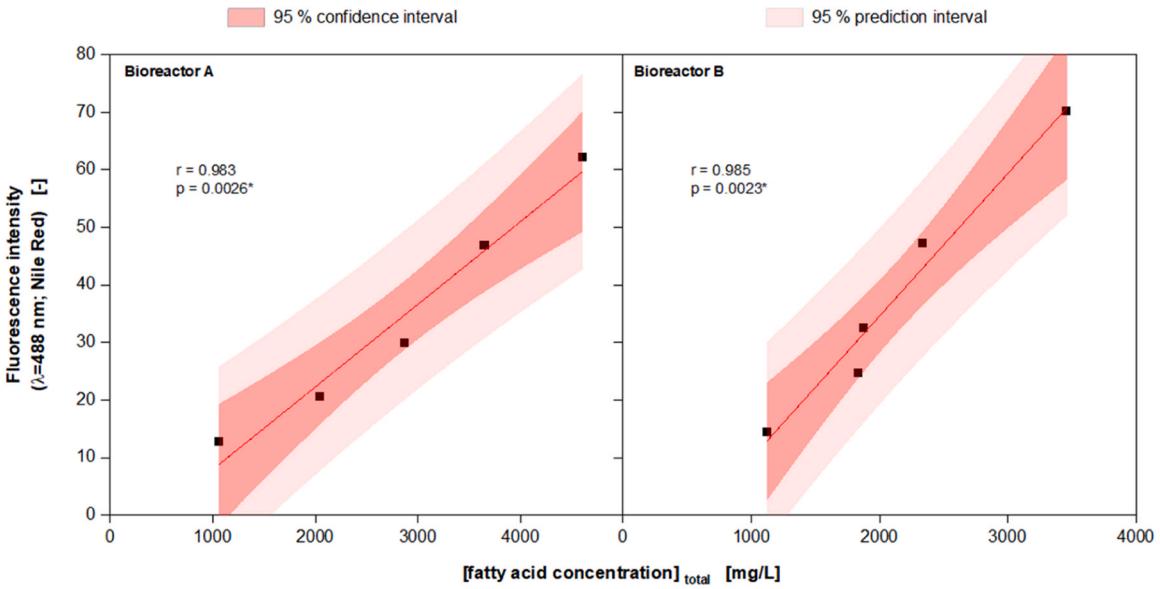

Fig. 5. : Correlation analysis of the total intracellular long-chain fatty acid concentration in *Y. lipolytica* S11070 cells, as determined by gas chromatography, and the fluorescence intensity induced by Nile Red bound to cellular, majorly LD-situated neutral lipids as determined with flow cytometry. Sampling points were at 8.38 h, 14.38 h, 20.38 h, 26.38 h, 32.38 h, and 44.63 h of cultivation time. Statistical evaluation was performed by a Pearson's correlation analysis and a two-sided significance test. r = Pearson correlation coefficient, p = probability value. *Statistical significance at $p < 0.005$.

images.

Interferometric techniques like 3D-DHM provide a variety of quantitatively determined optical parameters (Rappaz et al., 2014), from which a few were identified to correlate with the results of intracellular lipid quantification by GC-FID: phase uniformity (degree of uniformity concerning phase of light over the cell surface), phase contrast (intensity contrast of the phase image between neighbouring pixels averaged over the cell surface) and optical volume (proportional to the cell volume and its refractive index). In total, at least 300 cells were analyzed per sample, and the median as well as the variance (measure for population heterogeneity) were calculated for each parameter. Among the considered parameters, the optical volume showed the statistically most relevant linear correlation to the total intracellular long-chain fatty acid (C16:0, $^{\Delta 9}$C16:1, C18:0, C18:1–3, C20:0) concentration (TFA - Fig. 6) as measured by gas chromatography (Fig. 3).

Indicated by p values $<< 0.001$, the correlations are of statistical relevance, as by definition $p < 0.005$ is regarded as the significance threshold for "new discoveries" in science (Benjamin et al., 2018). Besides, the physical explanation of the optical volume as a suitable measure for intracellular lipid accumulation is evident: the optical volume is a function derived from the optical path difference (OPD) between the light beam that passed the specimen (object beam) and the reference beam. This is directly proportional to the phase difference ϕ between the sample and reference waves:

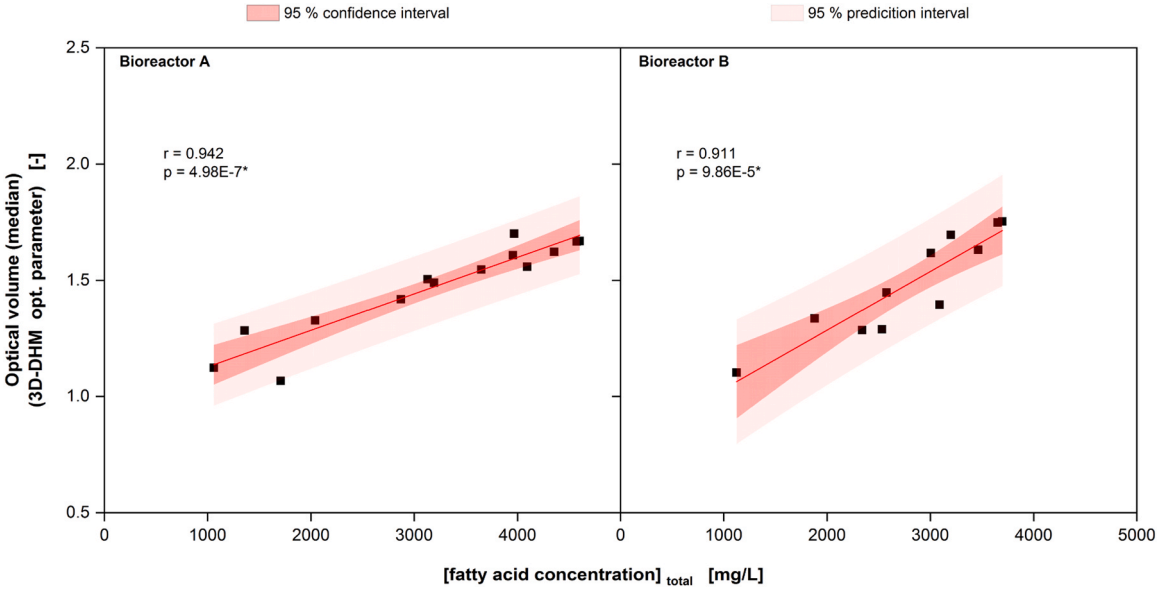

Fig. 6. : Correlation analysis of the total intracellular long-chain fatty acid concentration in *Y. lipolytica* S11070 cells, as determined by gas chromatography and the optical volume as determined by digital holographic microscopy. Sampling points were between 16.38 h and 46.63 h of cultivation time. Sample size was N > 300 cells per sampling point, n = 14 samples per bioreactor cultivation. Statistical evaluation was performed by Pearson correlation analysis and a two-sided significance test. r = Pearson correlation coefficient, p = probability value. *Statistically significant at $p < 0.005$.

$$OPD(p,q) = h \quad (p,q) \bullet [n_{cell} \quad (p,q) - n_m] \tag{1}$$

where $h(p,q)$ is the thickness of the sample for pixel (p,q) and $n_{cell}(p,q)$ is the integral refractive index distribution of the cell (Dardikman and Shaked, 2018). In summary, the optical volume is a function of the physical cell thickness and the (unknown) refractive index (RI) of the cell. This property is linked to the intracellular protein and water concentration (Rappaz et al., 2009, 2008). Long-chain fatty acids that are situated in lipid droplets have an RI that can be distinguished from the cytosol (Campos et al., 2018). Hence, they have an effect on the OPD. In general, all cellular content and compartments whose refractive indices significantly differ from that of water will have an influence on the optical volume. The obtained p-values of $p < 0.005$ between the intracellular lipid content and the optical volume of both, the wild-type (Fig. 6) and the lipid-overproducing (Fig. 8) *Y. lipolytica* strains demonstrate, however, that this contribution is negligible in this work: the correlations last from low to high lipid concentrations. Ultimately, a putative application of this method and correlation to other microorganisms remains to be elucidated though. The set-up-specific calibration of a (lipid quantification) method is, however, not unique to 3D-DHM, but is a pre-requisite for other analytical technologies like CARS (Wolinski et al., 2012; Wolinski and Kohlwein, 2015).

In analogy to the single-cell visualization of FCM (Fig. 4), intracellular total lipid accumulation in *Y. lipolytica* S11070 as determined via the cell optical volume through 3D-DHM – is shown in Fig. 7 in histogram plots. Between cultivation times of 8.38 h and 44.63 h, the optical volume (median) increased in both cultivations, which is in coherence with the findings of lipid accumulation as measured by GC (C16:0, $^{\Delta 9}$C16:1, C18:0, C18:1–3, C20:0; Fig. 3) and FCM (Fig. 4). This behavior was expected as the cytosolic refractive index of cells is increasing upon the accumulation of lipids in the cell interior, which in turn causes the optical volume to rise according to formula (1). In accordance with values from FCM-derived fluorescence intensity standard deviations (Table 4), the population heterogeneity as measured by 3D-DHM (variance of the optical volume, Fig. 7) is increasing during the course of the cultivation. The last sample (44.63 h) of bioreactor cultivation A (Fig. 6) shows the widest distribution of the side scatter – there is a higher portion of damaged cells, which do not follow the micromorphology patterns and are thus not recognized as cells by the automated image detection of 3D-DHM. This is seen as an asset as these cells remain unrecognized while they are hardly viable and do not contribute to the harvestable long-chain fatty acid amount.

The good correlation between optical parameters provided by the holographic microscope and the intracellular lipid concentration, as investigated in this work, proves 3D-DHM to be a suitable analytical technique for monitoring intracellular lipid accumulation in *Y. lipolytica*, as it had already been demonstrated for adipocytes (Campos et al., 2018) and algae (Marbà-Ardébol et al., 2017) before, although other optical features were used.

3.3.2. 3D-DHM analysis with an overproducing strain

The method was applied for a genetically engineered lipid overproducing strain as well in order to investigate the suitability at elevated intracellular lipid concentrations. The *Y. lipolytica* S11070 wild-type strain was modified to the lipid overproducing strain S15010, in which the lipase encoding *tgl4* gene was deficient. Medium and feeding strategy as well as analytical procedures were maintained in comparison to the cultivation with the wild-type strain. The results of the correlation analysis between the total long-chain fatty acid concentration as determined by GC-FID and by 3D-DHM are illustrated in Fig. 8. In comparison to the previous case, it was not possible to get access to a higher number of samples. The transferability of the method, however, is shown throughout the course of the cultivation.

The total intracellular long-chain fatty acid concentration increased from ca. 1,000 mg/L to 12,500 mg/L, equal to 160 mg/g_{CDW} to 360 mg/g_{CDW}. The maximum value is almost 2.5 times as high as that of wild-type strain S11070 (Fig. 3F). The correlation between the total long-chain fatty acid concentration and the optical volume remains to be statistically relevant ($p = 0.0044$), almost as good as the one obtained in cultivations with the wild-type strain (Fig. 6). Pearson correlation analysis yielded a positive, nearly full correlation with a coefficient of $r = 0.976$. This proves the methodology is valid at higher lipid accumulation in genetically modified organisms as well.

4. Conclusion and outlook

3D-DHM coupled to automated image and data analysis, was proven to be suitable for the fast, label-free and easy quantification of total intracellular lipid accumulation in oleaginous yeast *Y. lipolytica* bioreactor cultivation samples. Specific lipid contents between approximately 70 mg/g_{CDW} to 360 mg/g_{CDW} were analyzed on a single-cell basis, which also allows the investigation of population heterogeneity. It thus can replace or complement methods that rely on staining techniques or chromatographic analysis if the knowledge about the exact composition

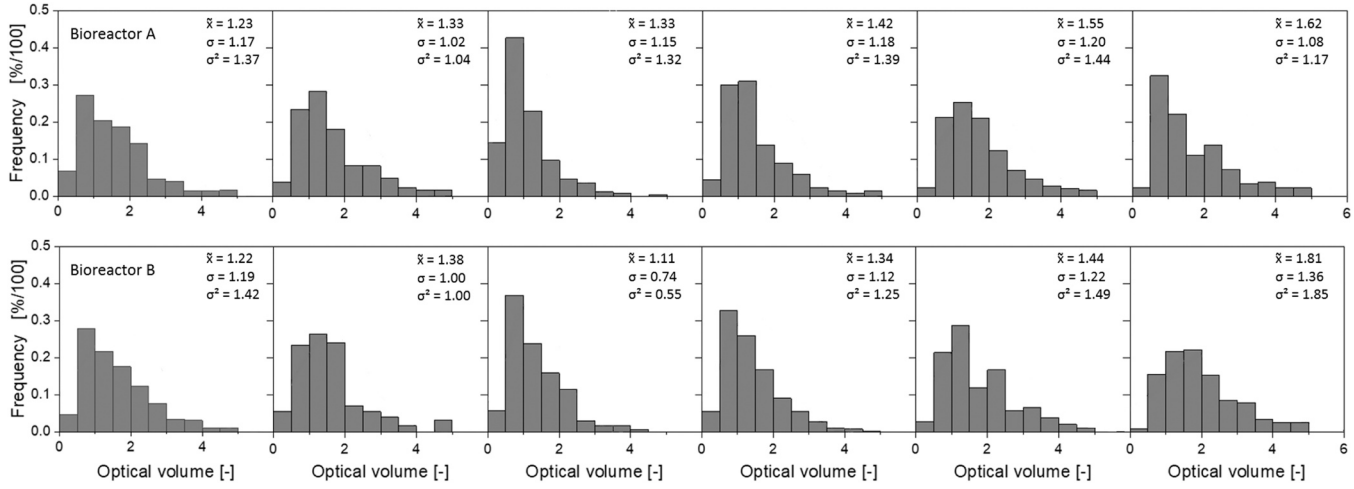

Fig. 7. : Optical cell volume distribution as determined by three-dimensional digital holographic microscopy of *Y. lipolytica* S11070 cells. This optical parameter is dependent on the physical cell volume and the cytosolic refractive index, with both these parameters increasing in the course of intracellular lipid accumulation. At least N = 300 cells per sample measured, displayed in a relative parametric distribution. Upper row represents values of bioreactor A, lower row represents values of bioreactor B. Samples of following timepoints were examined: column 1: 8.38 h, column 2: 14.38 h, column 3: 20.38 h, column 4: 26.38 h, column 5: 32.38 h, column 6: 44.63 h. $\tilde{x}$ = median, σ = standard deviation, σ^2 = variance.

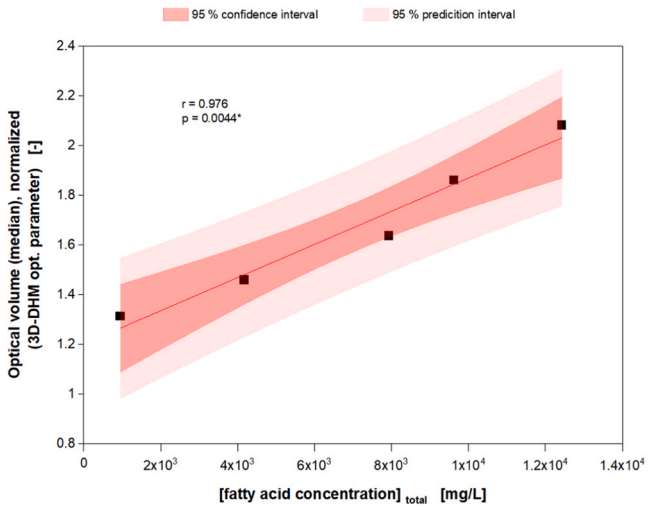

Fig. 8. : Correlation analysis of the total intracellular long-chain fatty acid concentration in *Y. lipolytica* S15010 lipid overproducing cells as determined by gas chromatography, and the optical volume as determined by digital holographic microscopy. Sampling points between 22.6 h and 52.8 h of cultivation time. Sample size was N > 250 cells per sampling point, n = 5 samples. Statistical evaluation was performed by a Pearson's correlation analysis and a two-sided significance test. r = Pearson correlation coefficient, p = probability value. *Statistically significant at $p < 0.005$.

of long-chain fatty acids is not the main interest. Due to the features of the optical volume, which considers the change of optical characteristics while lipids are accumulated intracellularly, it might be applicable to other microorganisms of similar size even if lipid accumulation does not happen in one single drop. The so far commercialized technology of 3D-DHM has already been combined with flow cells in such a way that a bypass measurement becomes feasible. The method, in principle, can be coupled to automated dilution, in order to obtain measurement precision and identifiability of single cells, while *real-time* measurements are achieved. It was shown recently that coupling DHM with a microfluidic cell and computation allowed the segregation and quantification of cellular compartments in *S. cerevisiae* (Bianco et al., 2023). Since macromorphology is changing in environmental stress conditions in *Y. lipolytica* (Timoumi et al., 2018), the methodology might be suitable to consider also the length-to-diameter ratio to investigate the impact of macromorphological changes on the individual long-chain fatty acid accumulation in cells and provide data about the physiological cell status. Any further automation will allow to gain more data for ensuring statistical validity and significance of the presented methodology.

CRediT authorship contribution statement

Simon Carl-Philipp Briel: Writing – original draft, Visualization, Methodology, Investigation. **Eva Johanna Moldenhauer:** Methodology, Investigation. **Nicolas Feuser:** Writing – review & editing, Methodology, Investigation. **Peter Neubauer:** Writing – review & editing, Supervision, Resources, Funding acquisition, Conceptualization. **Johannes Kabisch:** Writing – review & editing, Resources, Methodology. **Stefan Junne:** Writing – review & editing, Supervision, Resources, Project administration, Methodology, Funding acquisition, Conceptualization.

Declaration of Competing Interest

The authors declare that they have no known competing financial interests or personal relationships that could have appeared to influence the work reported in this paper.

Acknowledgements

This work was supported by the German Federal Ministry of Education and Research within the ERA-Net framework program ERA CoBioTech, project "Scale-App", grant no. 031B0622B.

Appendix

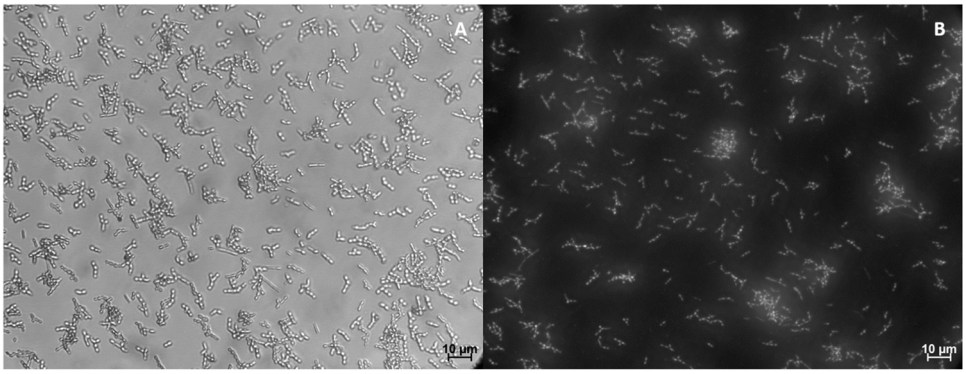

Figure A1. Fluorescence image microscopy of *Y. lipolytica* S11070 cells after Nile Red staining according to the protocol as described in material & methods. (A) shows a brightfield microscopic image without the application of a filter, (B) shows the same image with a fluorescent filter with a passband between 663 and 738 nm applied. Samples were drawn from the bioreactor ~20 h after inoculation. For image acquisition, a Nikon Eclipse Ti2 inverted microscope (Nikon Instruments, Tokyo, Japan) was applied.

Data Availability

Data will be made available on request.

References

Benjamin, D.J., Berger, J.O., Johannesson, M., Nosek, B.A., Wagenmakers, E.-J., Berk, R., Bollen, K.A., Brembs, B., Brown, L., Camerer, C., Cesarini, D., Chambers, C.D., Clyde, M., Cook, T.D., De Boeck, P., Dienes, Z., Dreber, A., Easwaran, K., Efferson, C., Fehr, E., Fidler, F., Field, A.P., Forster, M., George, E.I., Gonzalez, R., Goodman, S., Green, E., Green, D.P., Greenwald, A.G., Hadfield, J.D., Hedges, L.V., Held, L., Hua

Ho, T., Hoijtink, H., Hruschka, D.J., Imai, K., Imbens, G., Ioannidis, J.P.A., Jeon, M., Jones, J.H., Kirchler, M., Laibson, D., List, J., Little, R., Lupia, A., Machery, E., Maxwell, S.E., McCarthy, M., Moore, D.A., Morgan, S.L., Munafó, M., Nakagawa, S., Nyhan, B., Parker, T.H., Pericchi, L., Perugini, M., Rouder, J., Rousseau, J., Savalei, V., Schönbrodt, F.D., Sellke, T., Sinclair, B., Tingley, D., Van Zandt, T., Vazire, S., Watts, D.J., Winship, C., Wolpert, R.L., Xie, Y., Young, C., Zinman, J., Johnson, V.E., 2018. Redefine statistical significance. Nat. Hum. Behav. 2, 6–10. https://doi.org/10.1038/s41562-017-0189-z.

Beopoulos, A., Mrozova, Z., Thevenieau, F., Le Dall, M.T., Hapala, I., Papanikolaou, S., Chardot, T., Nicaud, J.M., 2008. Control of lipid accumulation in the yeast *Yarrowia lipolytica*. Appl. Environ. Microbiol. 74, 7779–7789. https://doi.org/10.1128/AEM.01412-08.

Beopoulos, A., Cescut, J., Haddouche, R., Uribelarrea, J.L., Molina-Jouve, C., Nicaud, J. M., 2009. *Yarrowia lipolytica* as a model for bio-oil production. Prog. Lipid Res. 48, 375–387. https://doi.org/10.1016/j.plipres.2009.08.005.

Bianco, V., D'Agostino, M., Pirone, D., Giugliano, G., Mosca, N., Di Summa, M., Scerra, G., Memmolo, P., Miccio, L., Russo, T., Stella, E., Ferraro, P., 2023. Label-free intracellular multi-specificity in yeast cells by phase-contrast tomographic flow cytometry. Small Methods 7. https://doi.org/10.1002/smtd.202300447.

Blazeck, J., Hill, A., Liu, L., Knight, R., Miller, J., Pan, A., Otoupal, P., Alper, H.S., 2014. Harnessing *Yarrowia lipolytica* lipogenesis to create a platform for lipid and biofuel production. Nat. Commun. 5, 1–10. https://doi.org/10.1038/ncomms4131.

Boltyanskiy, R., Odete, M.A., Cheong, F.C., Philips, L.A., 2022. Label-free viability assay using *in-line* holographic video microscopy. Sci. Rep. 12, 12746. https://doi.org/10.1038/s41598-022-17098-y.

Boulton, C.A., Ratledge, C., 1981. Correlation of lipid accumulation in yeasts with possession of ATP: citrate lyase. Microbiology 127, 169–176. https://doi.org/10.1099/00221287-127-1-169.

Bruder, S., Moldenhauer, E.J., Lemke, R.D., Ledesma-Amaro, R., Kabisch, J., 2019. Drop-in biofuel production using fatty acid photodecarboxylase from *Chlorella variabilis* in the oleaginous yeast *Yarrowia lipolytica*. Biotechnol. Biofuels 12, 1–72. https://doi.org/10.1186/s13068-019-1542-4.

Bruder, S., Melcher, F.A., Zoll, T., Hackenschmidt, S., Kabisch, J., 2020. Evaluation of a *Yarrowia lipolytica* strain collection for its lipid and carotenoid production capabilities. Eur. J. Lipid Sci. Technol. 122, 1900172. https://doi.org/10.1002/ejlt.201900172.

Campos, V., Rappaz, B., Kuttler, F., Turcatti, G., Naveiras, O., 2018. High-throughput, nonperturbing quantification of lipid droplets with digital holographic microscopy. J. Lipid Res. 59, 1301–1310. https://doi.org/10.1194/jlr.D085217.

Carsanba, E., Papanikolaou, S., Fickers, P., Erten, H., 2020. Lipids by *Yarrowia lipolytica* strains cultivated on glucose in batch cultures. Microorganisms 8, 1–14. https://doi.org/10.3390/microorganisms8071054.

Chmielarz, M., Sampels, S., Blomqvist, J., Brandenburg, J., Wende, F., Sandgren, M., Passoth, V., 2019. FT-NIR: A tool for rapid intracellular lipid quantification in oleaginous yeasts. Biotechnol. Biofuels 12, 169. https://doi.org/10.1186/s13068-019-1513-9.

Cooper, M.S., Hardin, W.R., Petersen, T.W., Cattolico, R.A., 2010. Visualizing "green oil" in live algal cells. J. Biosci. Bioeng. 109, 198–201. https://doi.org/10.1016/j.jbiosc.2009.08.004.

Dardikman, G., Shaked, N.T., 2018. Review on methods of solving the refractive index–thickness coupling problem in digital holographic microscopy of biological cells. Opt. Commun. 422, 8–16. https://doi.org/10.1016/J.OPTCOM.2017.11.084.

De la Hoz Siegler, H., Ayidzoe, W., Ben-Zvi, A., Burrell, R.E., McCaffrey, W.C., 2012. Improving the reliability of fluorescence-based neutral lipid content measurements in microalgal cultures. Algal Res. 1, 176–184. https://doi.org/10.1016/j.algal.2012.07.004.

Delvigne, F., Zacchetti, B., Fickers, P., Fifani, B., Roulling, F., Lefebvre, C., Neubauer, P., Junne, S., 2018. Improving control in microbial cell factories: from single-cell to large-scale bioproduction. FEMS Microbiol. Lett. 365. https://doi.org/10.1093/femsle/fny236.

Dulermo, T., Lazar, Z., Dulermo, R., Rakicka, M., Haddouche, R., Nicaud, J.-M., 2015. Analysis of ATP-citrate lyase and malic enzyme mutants of *Yarrowia lipolytica* points out the importance of mannitol metabolism in fatty acid synthesis. Biochim. Et Biophys. Acta (BBA) - Mol. Cell Biol. Lipids 1851, 1107–1117. https://doi.org/10.1016/j.bbalip.2015.04.007.

Encarnação, T., Arranja, C.T., Cova, T.F.G.G., Pais, A.A.C.C., Campos, M.G., Sobral, A.J. F.N., Burrows, H.D., 2018. Monitoring oil production for biobased feedstock in the microalga *Nannochloropsis* sp.: a novel method combining the BODIPY BD-C12 fluorescent probe and simple image processing. J. Appl. Phycol. 30, 2273–2285. https://doi.org/10.1007/s10811-018-1437-y.

Esmonde-White, K.A., Cuellar, M., Lewis, I.R., 2022. The role of Raman spectroscopy in biopharmaceuticals from development to manufacturing. Anal. Bioanal. Chem. 414, 969–991. https://doi.org/10.1007/s00216-021-03727-4.

Evans, C.T., Scragg, A.H., Ratledge, C., 1983. A comparative study of citrate efflux from mitochondria of oleaginous and non-oleaginous yeasts. Eur. J. Biochem. 130, 195–204. https://doi.org/10.1111/j.1432-1033.1983.tb07136.x.

Gatter, M., Förster, A., Bär, K., Winter, M., Otto, C., Petzsch, P., Ježková, M., Bahr, K., Pfeiffer, M., Matthäus, F., Barth, G., 2014. A newly identified fatty alcohol oxidase gene is mainly responsible for the oxidation of long-chain ω-hydroxy fatty acids in *Yarrowia lipolytica*. FEMS Yeast Res. 14, 858–872. https://doi.org/10.1111/1567-1364.12176.

González-García, Y., Rábago-Panduro, L.M., French, T., Camacho-Córdova, D.I., Gutiérrez-González, P., Córdova, J., 2017. High lipids accumulation in *Rhodosporidium toruloides* by applying single and multiple nutrients limitation in a simple chemically defined medium. Ann. Microbiol. 67, 519–527. https://doi.org/10.1007/s13213-017-1282-2.

Govender, T., Ramanna, L., Rawat, I., Bux, F., 2012. BODIPY staining, an alternative to the Nile Red fluorescence method for the evaluation of intracellular lipids in microalgae. Bioresour. Technol. 114, 507–511. https://doi.org/10.1016/j.biortech.2012.03.024.

Greenspan, P., Fowler, S.D., 1985. Spectrofluorometric studies of the lipid probe, nile red. J. Lipid Res. 26, 781–789. https://doi.org/10.1016/S0022-2275(20)34307-8.

Gupta, A., Dorlhiac, G.F., Streets, A.M., 2019. Quantitative imaging of lipid droplets in single cells. Analyst 144, 753–765. https://doi.org/10.1039/c8an01525b.

Hackenschmidt, S., Bracharz, F., Daniel, R., Thürmer, A., Bruder, S., Kabisch, J., 2019. Effects of a high-cultivation temperature on the physiology of three different *Yarrowia lipolytica* strains. FEMS Yeast Res. 19. https://doi.org/10.1093/femsyr/foz068.

Hillig, F., Annemüller, S., Chmielewska, M., Pilarek, M., Junne, S., Neubauer, P., 2013. Bioprocess development in single-use systems for heterotrophic marine microalgae. Chem. Ing. Tech. 85, 153–161. https://doi.org/10.1002/cite.201200143.

Hwang, J.-H., Choi, C.S., 2015. Use of *in vivo* magnetic resonance spectroscopy for studying metabolic diseases. Exp. Mol. Med. 47, e139. https://doi.org/10.1038/emm.2014.101.

Junne, S., Kabisch, J., 2017. Fueling the future with biomass: processes and pathways for a sustainable supply of hydrocarbon fuels and biogas. Eng. Life Sci. 17, 14–26. https://doi.org/10.1002/elsc.201600112.

Kamineni, A., Shaw, J., 2020. Engineering triacylglycerol production from sugars in oleaginous yeasts. Curr. Opin. Biotechnol. 62, 239–247. https://doi.org/10.1016/j.copbio.2019.12.022.

Kennedy, E.P., 1961. Biosynthesis of complex lipids. Fed. Proc. 20, 934–940.

Kimura, K., Yamaoka, M., Kamisaka, Y., 2004. Rapid estimation of lipids in oleaginous fungi and yeasts using Nile red fluorescence. J. Microbiol. Methods 56, 331–338. https://doi.org/10.1016/j.mimet.2003.10.018.

Kochan, K., Peng, H., Wood, B.R., Haritos, V.S., 2018. Single cell assessment of yeast metabolic engineering for enhanced lipid production using Raman and AFM-IR imaging. Biotechnol. Biofuels 11, 106. https://doi.org/10.1186/s13068-018-1108-x.

Kolouchová, I., Maťátková, O., Sigler, K., Masák, J., Řezanka, T., 2016. Lipid accumulation by oleaginous and non-oleaginous yeast strains in nitrogen and phosphate limitation. Fol. Microbiol. 61. https://doi.org/10.1007/s12223-016-0454-y.

Kukal, G., Vasdekis, A.E., McDonald, A.G., 2022. Raman-probes for monitoring metabolites and nutrient fate in *Yarrowia lipolytica* using deuterated glucose. Biocatal. Agric. Biotechnol. 39, 102241. https://doi.org/10.1016/j.bcab.2021.102241.

Kyle, D., Ratledge, C., Ratledge, C., 1992. Microbial Lipids. In: Rehm, H.-J., Reed, G. (Eds.), Industrial Applications of Single Cell Oils. VCH Verlagsgesellschaft mbH, Hull, UK, pp. 135–197. https://doi.org/10.1201/9781439821855.ch1.

Lazar, Z., Dulermo, T., Neuvéglise, C., Crutz-Le Coq, A.-M., Nicaud, J.-M., 2014. Hexokinase-A limiting factor in lipid production from fructose in *Yarrowia lipolytica*. Metab. Eng. 26, 89–99. https://doi.org/10.1016/j.ymben.2014.09.008.

Lei, Y., Wang, X., Sun, S., He, B., Sun, W., Wang, K., Chen, Z., Guo, Z., Li, Z., 2024. A review of lipid accumulation by oleaginous yeasts: culture mode. Sci. Total Environ. 919, 170385. https://doi.org/10.1016/j.scitotenv.2024.170385.

Lemoine, A., Delvigne, F., Bockisch, A., Neubauer, P., Junne, S., 2017. Tools for the determination of population heterogeneity caused by inhomogeneous cultivation conditions. J. Biotechnol. 251. https://doi.org/10.1016/j.jbiotec.2017.03.020.

Lorenz, E., Runge, D., Marbà-Ardébol, A.-M., Schmacht, M., Stahl, U., Senz, M., 2017. Systematic development of a two-stage fed-batch process for lipid accumulation in *Rhodotorula glutinis*. J. Biotechnol. 246, 4–15. https://doi.org/10.1016/j.jbiotec.2017.02.010.

Maczek, J., Junne, S., Nowak, P., Goetz, P., 2006. Metabolic flux analysis of the sterol pathway in the yeast *Saccharomyces cerevisiae*. Bioprocess Biosyst. Eng. 29, 241–252. https://doi.org/10.1007/s00449-006-0072-1.

Marbà-Ardébol, A.-M., Emmerich, J., Neubauer, P., Junne, S., 2017. Single-cell-based monitoring of fatty acid accumulation in *Crypthecodinium cohnii* with three-dimensional holographic and *in situ* microscopy. Process Biochem. 52, 223–232. https://doi.org/10.1016/j.procbio.2016.11.003.

Midtvedt, D., Olsén, E., Höök, F., Jeffries, G.D.M., 2019. Label-free spatio-temporal monitoring of cytosolic mass, osmolarity, and volume in living cells. Nat. Commun. 10, 340. https://doi.org/10.1038/s41467-018-08207-5.

Němcová, A., Gonová, D., Samek, O., Sipiczki, M., Breierová, E., Márová, I., 2021. The use of Raman spectroscopy to monitor metabolic changes in stressed *Metschnikowia* sp. yeasts. Microorganisms 9, 277. https://doi.org/10.3390/microorganisms9020277.

Ochoa-Estopier, A., Guillouet, S.E., 2014. D-stat culture for studying the metabolic shifts from oxidative metabolism to lipid accumulation and citric acid production in *Yarrowia lipolytica*. J. Biotechnol. 170, 35–41. https://doi.org/10.1016/j.jbiotec.2013.11.008.

Omelchenko, A.N., Okotrub, K.A., Surovtsev, N.V., 2023. Raman spectroscopy of yeast cells cultured on a deuterated substrate. Spectrochim. Acta A Mol. Biomol. Spectrosc. 303, 123262. https://doi.org/10.1016/j.saa.2023.123262.

Papanikolaou, S., Aggelis, G., 2009. Biotechnological valorization of biodiesel derived glycerol waste through production of single cell oil and citric acid by *Yarrowia lipolytica*. Lipid Technol. 21, 83–87. https://doi.org/10.1002/lite.200900017.

Papanikolaou, S., Aggelis, G., 2011. Lipids of oleaginous yeasts. Part I: biochemistry of single cell oil production. Eur. J. Lipid Sci. Technol. 113, 1031–1051. https://doi.org/10.1002/ejlt.201100014.

Patel, A., Mikes, F., Bühler, S., Matsakas, L., 2018. Valorization of Brewers' spent grain for the production of lipids by oleaginous yeast. Molecules. https://doi.org/10.3390/molecules23123052.

Patel, A., Antonopoulou, I., Enman, J., Rova, U., Christakopoulos, P., Matsakas, L., 2019. Lipids detection and quantification in oleaginous microorganisms: an overview of the current state of the art. BMC Chem. Eng. 1, 13. https://doi.org/10.1186/s42480-019-0013-9.

Princová, J., Schätz, M., Ťupa, O., Převorovský, M., 2019. Analysis of lipid droplet content in fission and budding yeasts using automated image processing. J. Vis. Exp. 149, e59889. https://doi.org/10.3791/59889.

Rakicka, M., Lazar, Z., Dulermo, T., Fickers, P., Nicaud, J.M., 2015. Lipid production by the oleaginous yeast *Yarrowia lipolytica* using industrial by-products under different culture conditions. Biotechnol. Biofuels 8, 104. https://doi.org/10.1186/s13068-015-0286-z.

Rappaz, B., Barbul, A., Emery, Y., Korenstein, R., Depeursinge, C., Magistretti, P.J., Marquet, P., 2008. Comparative study of human erythrocytes by digital holographic microscopy, confocal microscopy, and impedance volume analyzer. Cytom. Part A 73A, 895–903. https://doi.org/10.1002/cyto.a.20605.

Rappaz, B., Cano, E., Colomb, T., Kuhn, J., Depeursinge, C., Simanis, V., Magistretti, P.J., Marquet, P., 2009. Noninvasive characterization of the fission yeast cell cycle by monitoring dry mass with digital holographic microscopy. J. Biomed. Opt. 14, 034049. https://doi.org/10.1117/1.3147385.

Rappaz, B., Breton, B., Shaffer, E., Turcatti, G., 2014. Digital holographic microscopy: a quantitative label-free microscopy technique for phenotypic screening. Comb. Chem. High. Throughput Screen. 17, 80–88. https://doi.org/10.2174/1386207313166660062.

Ratledge, C., 1993. Single cell oils - have they a biotechnological future? Trends Biotechnol. 11, 278–284. https://doi.org/10.1016/0167-7799(93)90015-2.

Ratledge, C., 1994. Yeasts, moulds, algae and bacteria as sources of lipids. In: Kamel, B. S., Kakuda, Y. (Eds.), Technological Advances in Improved and Alternative Sources of Lipids. Springer US, Boston, MA, pp. 235–291. https://doi.org/10.1007/978-1-4615-2109-9_9.

Ratledge, C., Wynn, J.P., 2002b. The Biochemistry and Molecular Biology of Lipid Accumulation in Oleaginous Microorganisms. In: Laskin, A.I., Bennet, J.W., Gadd, G. M. (Eds.), Advances in Applied Microbiology, 51. Academic Press, London, p. 1. https://doi.org/10.1016/S0065-2164(02)51000-5.

Rumin, J., Bonnefond, H., Saint-Jean, B., Rouxel, C., Sciandra, A., Bernard, O., Cadoret, J.-P., Bougaran, G., 2015. The use of fluorescent Nile red and BODIPY for lipid measurement in microalgae. Biotechnol. Biofuels 8, 42. https://doi.org/10.1186/s13068-015-0220-4.

Sanborn, D., He, R., Feng, L., Hong, J., 2023. *In situ* biological particle analyzer based on digital inline holography. Biotechnol. Bioeng. 120, 1399–1410. https://doi.org/10.1002/bit.28338.

Sokoła-Wysoczańska, E., Wysoczański, T., Wagner, J., Czyż, K., Bodkowski, R., Lochyński, S., Patkowska-Sokoła, B., 2018. Polyunsaturated fatty acids and their potential therapeutic role in cardiovascular system disorders-a review. Nutrients 10, 1561. https://doi.org/10.3390/nu10101561.

Taeuber, S., Cziommer, J., Neubauer, P., Junne, S., 2021. From cellulose to lipids. In: Aresta, M., Dibenedetto, A., Dumeignil, F. (Eds.), Biorefinery: From Biomass to Chemicals and Fuels. De Gruyter. https://doi.org/10.1515/9783110705386.

Thorpe, R.F., Ratledge, C., 1972. Fatty Acid Distribution in Triglycerides of Yeasts Grown on Glucose or n-Alkanes. J. Gen. Microbiol. 72, 151–163. https://doi.org/10.1099/00221287-72-1-151.

Timoumi, A., Guillouet, S.E., Molina-Jouve, C., Fillaudeau, L., Gorret, N., 2018. Impacts of environmental conditions on product formation and morphology of *Yarrowia lipolytica*. Appl. Microbiol. Biotechnol. https://doi.org/10.1007/s00253-018-8870-3.

Wieland, K., Masri, M., von Poschinger, J., Brück, T., Haisch, C., 2021. Non-invasive Raman spectroscopy for time-resolved *in-line* lipidomics. RSC Adv. 11, 28565–28572. https://doi.org/10.1039/D1RA04254H.

Wolinski, H., Kohlwein, S.D., 2008. Microscopic analysis of lipid droplet metabolism and dynamics in yeast. Methods Mol. Biol. 151–163. https://doi.org/10.1007/978-1-59745-261-8_11.

Wolinski, H., Kohlwein, S.D., 2015. Microscopic and spectroscopic techniques to investigate lipid droplet formation and turnover in yeast. In: Tang, B.L. (Ed.), Membrane Trafficking, Second Edition. Humana Press, New York, NY, pp. 289–305. https://doi.org/10.1007/978-1-4939-2309-0_21.

Wolinski, H., Bredies, K., Kohlwein, S.D., 2012. Quantitative imaging of lipid metabolism in yeast: from 4D analysis to high content screens of mutant libraries. In: Di Paolo, G., Wenk, M.R. (Eds.), Methods in Cell Biology. Elsevier Inc, pp. 345–365. https://doi.org/10.1016/B978-0-12-386487-1.00016-X.

Xie, D., Jackson, E.N., Zhu, Q., 2015. Sustainable source of omega-3 eicosapentaenoic acid from metabolically engineered *Yarrowia lipolytica*: from fundamental research to commercial production. Appl. Microbiol. Biotechnol. 99, 1599–1610. https://doi.org/10.1007/s00253-014-6318-y.

Yan, C.-X., Zhang, Y., Yang, W.-Q., Ma, W., Sun, X.-M., Huang, H., 2024. Universal and unique strategies for the production of polyunsaturated fatty acids in industrial oleaginous microorganisms. Biotechnol. Adv. 70, 108298. https://doi.org/10.1016/j.biotechadv.2023.108298.

Yourassowsky, C., Theunissen, R., Dohet-Eraly, J., Dubois, F., 2024. Lipid quantification in living microalgal cultures with digital holographic microscopy. Front. Photonics 4. https://doi.org/10.3389/fphot.2023.1301708.

Zhang, H., Zhang, L., Chen, H., Chen, Y.Q., Ratledge, C., Song, Y., Chen, W., 2013. Regulatory properties of malic enzyme in the oleaginous yeast, *Yarrowia lipolytica*, and its non-involvement in lipid accumulation. Biotechnol. Lett. 35, 2091–2098. https://doi.org/10.1007/s10529-013-1302-7.